Evidence for β Scission in the Oxidation of Amino Acids

Pawel Wisniowski,[†,‡] Ian Carmichael,[†] Richard W. Fessenden,[†] and Gordon L. Hug*[,†]

Radiation Laboratory, University of Notre Dame, Notre Dame, Indiana 46556, and Department of Radiation Chemistry and Technology, Institute of Nuclear Chemistry and Technology, Dorodna 16, 03-195 Warsaw, Poland

Received: October 24, 2001; In Final Form: January 18, 2002

Time-resolved ESR and steady-state spin trapping were used to identify the radicals and their kinetics following the radiolytic oxidation by the •OH radical of the anion of α-methylalanine, $H_2N-C(CH_3)_2-CO_2^-$. Spectra of two new radicals were identified in aqueous solution, the aminyl radical, $HN^{\bullet}-C(CH_3)_2-CO_2^-$, and the decarboxylated radical, $H_2N-{}^{\bullet}C(CH_3)_2$. Time-resolved ESR spectra of the two new radicals were obtained, and the hyperfine couplings and *g* factors were determined. The radical formation times were consistent with both of the radicals being formed in the initial attack of the •OH radical on α-methylalanine. Measurements of the radical yields indicated that the aminyl radical was the major radical product from the initial •OH attack. The observations (a) that the aminyl radical decays via a first-order process (lifetime about 14 μs) and (b) that there is a large presence of $^{\bullet}CO_2^-$ spin adducts with $CH_2{=}NO_2^-$ are consistent with β scission being a prominent reaction of the aminyl radical from α-methylalanine. Aspects of the radiolytic oxidations by the •OH of α-methylalanine and glycine are contrasted with respect to initial radical formation and the subsequent reactions of the resulting radicals. These experimental findings corroborate predictions from density functional theory calculations of prompt decarboxylation following electron loss from the α-methylalanine anion and preferential formation of the N-centered radical via H abstraction.

Introduction

The oxidation of simple amino acids by the •OH radical has turned out to be quite complicated. This finding is of significance to questions of how aminopolycarboxylic acids degrade (organic aging) in nuclear waste storage tanks.[1] The precise chemical mechanisms of amino acid oxidation are also of interest to understanding the fate of proteins under oxidative stress in biological systems.[2,3] Recently, a comprehensive scheme[4] for the oxidation of glycine anions was proposed that attempts to explain systematically all of the processes from subnanosecond to steady-state time scales. Of special note, several radicals were postulated as being involved in the beginning steps of glycine−anion oxidation.[4] The initial steps were seen as producing two main radicals, $H_2N^{\bullet+}-CH_2-CO_2^-$ and $HN^{\bullet}-CH_2-CO_2^-$:

$$^{\bullet}OH + H_2N-CH_2-CO_2^- \rightarrow H_2N^{\bullet+}-CH_2-CO_2^- + OH^- \quad (1)$$

$$^{\bullet}OH + H_2N-CH_2-CO_2^- \rightarrow HN^{\bullet}-CH_2-CO_2^- + H_2O \quad (2)$$

The zwitterion radical, $H_2N^{\bullet+}-CH_2-CO_2^-$, decarboxylates immediately

$$H_2N^{\bullet+}-CH_2-CO_2^- \rightarrow {}^{\bullet}CH_2NH_2 + CO_2 \quad (3)$$

according to the published scheme, but its conjugate base, the aminyl radical $HN^{\bullet}-CH_2-CO_2^-$, appeared to have a nonnegligible lifetime at high pH. That the aminyl radical does not rapidly protonate to the zwitterion radical and decarboxylate at high pH is consistent with an estimate[5] of the low $pK_a = 2.6$ of the zwitterion radical, leaving any aminyl radicals deprotonated at high pH.

It was recently shown by time-resolved ESR (TRESR)[6] that $H_2N-{}^{\bullet}CH-CO_2^-$ was also produced early in the process:

$$^{\bullet}OH + H_2N-CH_2-CO_2^- \rightarrow H_2N-{}^{\bullet}CH-CO_2^- + H_2O \quad (4)$$

In addition, the TRESR measurements detected rapid formation of $^{\bullet}CH_2NH_2$ radicals, and this observation lends indirect support for the aminium zwitterion radical, $H_2N^{\bullet+}-CH_2-CO_2^-$, being formed (reaction 1) and then decarboxylating (reaction 3) to yield the observed $^{\bullet}CH_2NH_2$ radicals as predicted from ab initio molecular orbital and density functional theory (DFT) calculations. Initially the presence of aminyl radicals, $HN^{\bullet}-CH_2-CO_2^-$, also predicted from theory, was only inferred from scavenging reactions with hydroquinones,[4] but they were subsequently identified in steady-state radiolysis experiments with the *aci*-anion ($CH_2{=}NO_2^-$) of nitromethane as a spin-trap.[7] The TRESR amplitudes of $^{\bullet}CH_2NH_2$ and $H_2N-{}^{\bullet}CH-CO_2^-$ were also used to determine their yields. It was found that those yields did not sum to 100% of that of •OH, so production of some of the aminyl radical was inferred.

The aminyl radicals appeared to play a more significant role when glycine was substituted with methyl groups.[8] β scission of the aminyl radicals, with the formation of $^{\bullet}CO_2^-$ radicals, was thought to be a significant decay channel for these radicals, especially for $HN^{\bullet}-C(CH_3)_2-CO_2^-$ formed from the anions, $H_2N-C(CH_3)_2-CO_2^-$, of 2-aminoisobutyric acid (α-methylalanine).[8]

$$HN^{\bullet}-C(CH_3)_2-CO_2^- \rightarrow HN{=}C(CH_3)_2 + {}^{\bullet}CO_2^- \quad (5)$$

* To whom correspondence should be addressed. E-mail: hug.1@nd.edu. Fax: (219) 631-8068.
† University of Notre Dame.
‡ Institute of Nuclear Chemistry and Technology.

10.1021/jp0139383 CCC: $22.00
Published on Web 04/17/2002

The radical $^{\bullet}CO_2^-$ has recently been observed in spin-trapping experiments with steady-state radiolysis of glycine itself,[9] and the mechanism for this formation of $^{\bullet}CO_2^-$ in glycine was later assigned to a β-scission process.[8] However, the evidence for the formation of aminyl radicals

$$^{\bullet}OH + H_2N-C(CH_3)_2-CO_2^- \rightarrow HN^{\bullet}-C(CH_3)_2-CO_2^- + H_2O \quad (6)$$

and β scission (reaction 5) in α-methylalanine was inferential and made in analogy with the findings in glycine.[8] The purpose of the current work is to find direct physical evidence for this aminyl radical chemistry using TRESR and also spin-trapping experiments involving an alkyl-substituted glycine (α-methylalanine). From these experiments, we have analyzed the data to (1) determine if aminyl radicals are produced in solution, (2) ascertain if these radicals decay via β scission, and (3) validate the predictions of the DFT calculations regarding the various possible oxidative degradation channels.

A study of the ESR spectrum observed with α-methylalanine under steady-state in situ radiolysis has been made.[10] ESR lines attributable to $NH_2-C(CH_3)(^{\bullet}CH_2)CO_2^-$ were seen

$$^{\bullet}OH + H_2N-C(CH_3)_2-CO_2^- \rightarrow NH_2-C(CH_3)(^{\bullet}CH_2)CO_2^- + H_2O \quad (7)$$

but no radicals left over from a decarboxylation were observed. (A spectrum initially assigned to the radical $HN^{\bullet}-C(CH_3)_2-CO_2^-$ was reported in that work, but this spectrum was subsequently shown[11] to be from $^{\bullet}N{=}C(CH_3)_2$, presumably produced in secondary reactions.) However, carbon dioxide has been determined to evolve in steady-state gamma radiolysis of α-methylalanine.[12] Thus, the radical corresponding to the decarboxylated fragment of α-methylalanine should be present, and it would be of interest to estimate the rate of decarboxylation from the appearance rate of any such radical fragments.

Aminyl radicals of the structure $R-^{\bullet}NH$ are not well-known, whereas those of the type $R-^{\bullet}N-R'$ have been studied in some detail.[13] The γ irradiation of frozen amines has produced spectra attributed to the former type in alkylamines[14,15] ($H_3C-^{\bullet}NH$ from methylamine, for example), and the species $HO_2CCH_2-^{\bullet}NH$ has been reported[16] from a glycine crystal γ irradiated and then UV photolyzed at 77 K. Thus, the approximate magnitudes of the hyperfine constants are known. Other related examples observed in solution include radicals such as $H_3CCH_2O-^{\bullet}NH$[17] and $^-O_2C-^{\bullet}NH$.[18] These latter examples are relevant in that, on the basis of the absence of detectable lines of the aminyl radical in the case of glycine solution, it was not clear how large the ESR line width might be for such a species.

Experimental Section

2-Aminoisobutyric acid (α-methylalanine) was purchased from Aldrich. Anhydrous sodium sulfite was obtained from Mallinckrodt, and potassium hydroxide was obtained from Fisher Scientific. Nitromethane (99%) was from Aldrich. All of these chemicals were used without further purification. The deionized water was purified in a reverse osmosis/deionization system from a Serv-A-Pure Co. There is an UV-irradiation unit in the circulating section of this water-purification system. The purity of the water exceeds that of triply distilled water. It has a resistance >18 Mohm/cm and a total organic carbon (TOC) content of <10 ppb.

Radiolysis was carried out with electrons from a Van de Graaff accelerator. The chemical samples were contained in a quartz cell of 0.4 mm thickness, and the cell was irradiated edge-on. The solution to be irradiated was passed through a heat-exchange unit before entering the ESR cell in order to cool the solution so that formation of N_2O bubbles could be avoided. The measurements were made at a temperature of about 288 K. A bubble trap[19] was also used in most of the experiments. In the irradiated N_2O-saturated aqueous solutions, hydrated electrons, e_{aq}^-, are rapidly converted into $^{\bullet}OH$ by the reactions

$$H_2O \rightsquigarrow e_{aq}^-, {}^{\bullet}OH, H, H^+ \quad (8)$$

$$e_{aq}^- + N_2O \rightarrow N_2 + O^{\bullet -} \quad (9)$$

$$O^{\bullet -} + H_2O \rightarrow {}^{\bullet}OH + OH^- \; pK_a = 11.9 \quad (10)$$

The radiation doses and corresponding initial radical concentrations could be varied by adjusting the electron-beam current. All experiments used 10 mM solutions of α-methylalanine at pH 11.

Time-Resolved Experiments. In the pulsed mode of the Van de Graaff accelerator, typical conditions corresponded to an initial concentration of hydroxyl radicals, $^{\bullet}OH$, in the range of 40−50 μM in the N_2O-saturated aqueous solutions. The accelerator supplied 2.8 MeV electron pulses of ≈0.5 μs duration to the flowing aqueous solutions. The in situ time-resolved ESR equipment was described previously.[20−22] The TRESR was operated in both the kinetic-profile and the boxcar modes. Both of these modes are based on obtaining kinetic profiles with no frequency modulation.[23] The signal-averaged data are accumulated by summing pairs of matched kinetic traces. One trace in each pair is acquired at the nominal external magnetic field. The matching trace is acquired at a magnetic field that is shifted to a spectral position where no ESR absorption is located (ideally, at least in the kinetic-profile mode). This field shift is produced by a current through external coils on the cavity. These on- and off-resonance traces are subtracted, and the procedure is repeated with each intermediate result being folded into the average. Typical field steps were 1.5−4 G. The solution was flowed to avoid product build-up; the rate was typically 15 cm^3 min^{-1}.

The boxcar-scanning mode of operation of the ESR spectrometer has also been described previously.[22] In this mode, the external field is slowly scanned while the field is stepped between two values by the field coils. The data consists of the amplitude difference between the two magnetic fields for a selected time window. A number of data values are averaged, and the resultant value is sent through a D/A converter to a strip chart recorder. The external magnetic field is slowly scanned through a range to display a spectrum. Because the field steps are generally much smaller than in the kinetic-profile mode, the spectra have a first derivative form. To see broad lines, the field steps are taken to be relatively larger than is needed to see narrow lines. The magnetic field scale shown in the figures has its origin at a field defined by $g = 2.000\,43$ at the operating frequency of about 9351 MHz.

Yield Measurement. In the previous work on glycine,[7] a measurement of the yields of the several radical products was made from the amplitude of the TRESR kinetic traces. This method involved modeling the response by the use of modified Bloch equations and was also applied here. The ESR signal of $SO_3^{\bullet -}$ in N_2O-saturated sulfite solution was used as a reference, and the radical concentration was determined from the observed

second-order decay rate. The radical concentrations in other experiments were determined from the relative electron-beam current collected from the ESR cell. The microwave magnetic field was then determined from the period of the Torrey oscillations of the response of the high-field line of $^{-}O_2C$-$CH{=}C^{\bullet}CO_2^{-}$.[7,24] The observed line widths were determined from spectra taken by a point-to-point method. The width of the line of $^{-}O_2CCH{=}C^{\bullet}CO_2^{-}$ (which has large relaxation times) was used to determine the field inhomogeneity by modeling with the static magnetic resonance line shape convoluted with a Gaussian field inhomogeneity.[7] The observed line widths for other radicals were determined and used to give the T_2 values in a similar procedure. Corrections were made for partial overlap of the lines of $HN^{\bullet}-C(CH_3)_2-CO_2^{-}$ and $H_2N-^{\bullet}C(CH_3)_2$ within each spectrum. Because the lines of the aminyl radical are broader (0.5 G) than those of typical radicals ($\sim$0.05 G), the signal amplitudes are small so the error may be larger. Nevertheless, yield values of reasonable consistency were obtained. The error in an individual yield value is estimated to be of the order of 10%.

Spin Trapping. The spin-trapping experiments were done with the Van de Graaff accelerator in the steady-irradiation mode. In this mode of operation, the steady-state $[^{\bullet}OH]_{ss} \approx 1$ μM with the half-life of unscavenged $^{\bullet}OH \approx 300$ μs. The magnetic field was modulated at two frequencies, and successive synchronous detectors were used to provide a second-derivative presentation as the external magnetic field was scanned.[22] The spin-trap was the *aci*-anion of nitromethane, $CH_2{=}NO_2^{-}$. Radicals are trapped by radical addition to the carbon across the double bond, forming a radical of structure $RCH_2NO_2^{\bullet -}$. The basic spectrum consists of a 1:1:1 triplet produced by a nitrogen splitting on the order of 25 G with each of these lines further split into a 10 G 1:2:1 triplet by the protons of the CH_2 group. Any magnetic nuclei in the trapped species may add further small splittings.[25] The exact g factor and magnitude of all of the splittings depend on the group R.

Theoretical Section

Radical structures were determined by density functional theory (DFT) calculations using the popular B3LYP functional[26] and a polarized split-valence basis set, 6-31G(d,p),[27] augmented with diffuse functions on all "heavy" atoms, i.e., C, N, and O. Geometry optimizations were performed using analytic gradient techniques, and vibrational frequencies were determined from analytic Hessians to characterize the nature of the stationary points obtained. All calculations were performed with the Gaussian 98 series of programs.[28] Solvent effects were treated by application of the standard COSMO model[29] implemented in that package. More specific solute−solvent interactions were captured by a "supramolecular" approach, including explicit water molecules with and without surrounding dielectric media in a number of cases as discussed below. Hyperfine coupling parameters were determined by single-point calculations with a more flexible modified[30] double-ζ basis set, denoted [5s2p1d/3s1p], at the above geometries. Solvent effects on the magnetic parameters were evaluated by a similar computation at the solvent-optimized structure in the presence of the solvent reaction field.

Results and Discussion

Time-Resolved ESR in α-Methylalanine. When N_2O-saturated aqueous solutions of 10 mM α-methylalanine at pH 11 were pulse irradiated, the ESR amplitudes in the boxcar mode showed a spectrum such as that given in Figure 1. This spectrum

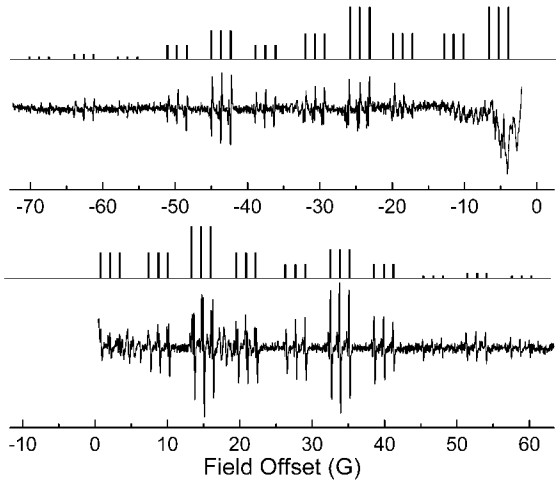

Figure 1. ESR spectrum taken during pulse radiolysis of a 10 mM solution of α-methylalanine at pH 11. The first-derivative presentation was obtained by use of the boxcar mode of the spectrometer. The sampling interval was from 1 to 4.2 μs after the end of the 0.6 μs radiolysis pulse, and the field step was about $\pm$ 40 mG. The field offset is from a position defined by $g = 2.00043$.

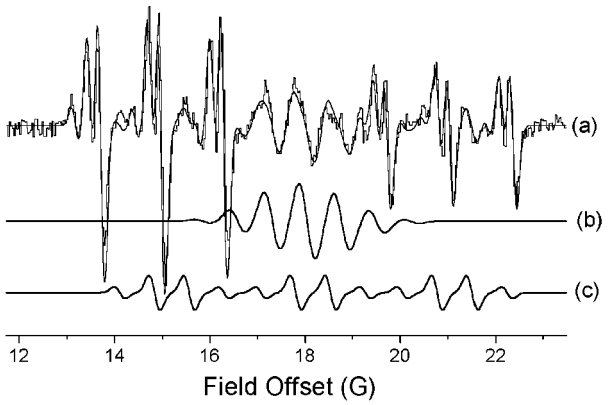

Figure 2. Expanded portion of the spectrum in Figure 1. The calculated first-derivative curve in b represents the lines expected for the aminyl radical and that in c is for the radical $NH_2-C(CH_3)(^{\bullet}CH_2)CO_2^{-}$. The full curve in a includes these two contributions as well as one for the lines of the radical $H_2N-^{\bullet}C(CH_3)_2$.

was collected in the time window of approximately 1.0−4.2 μs after the end of the irradiation pulse. The most intense lines in this spectrum are strongly polarized by chemically induced dynamic electron polarization (CIDEP) that results from the radical-pair mechanism. The low-field lines are in emission, and the high-field lines are in enhanced absorption. This is the typical E/A pattern found when singlet radical pairs react leaving triplet radical pairs. The lines in the center of the spectrum are hardly visible.

From Figure 1, the pattern consists of seven groups of lines with a splitting between the centers of adjacent groups of 18.90 G. A representation of the expected spectrum is shown by the "stick" spectrum. The pattern is indicative of six equivalent protons, and the expected second-order splitting is visible, see Figure 2. Furthermore, the intensities of seven main groups in Figure 1 are not inconsistent with the 1:6:15:20:15:6:1 ratio expected for six equivalent protons if account is taken of the spin polarization. Each of the seven major groups of lines is further split into a 6.06 G triplet (of intensities 1:2:1) by the two equivalent protons from the NH_2 group, and these lines are further split into 1:1:1 triplets produced by the nitrogen.

The central major group of lines (corresponding to relative intensity 20 for six equivalent protons) is of small intensity

TABLE 1: ESR Parameters[a]

radical	g	a_N	a_H(CH)	a_H(CH)	a_H(NH)
$HN^{\bullet}-C(CH_3)_2-CO_2^-$ [b]	2.00416	13.43		0.73 (6H)	22.30 (1H)
$H_2N-{}^{\bullet}C(CH_3)_2$ [c]	2.00274	1.32	18.90 (6H)		6.07 (2H)
$H_2NC(CH_3)({}^{\bullet}CH_2)CO_2^-$ [b]	2.00261[d]	2.97	21.89 (2H)	0.73 (3H)	

[a] Hyperfine constants in Gauss. The number of equivalent nuclei is given in parentheses. [b] The accuracy of the hyperfine constants is about ±0.05 G; the accuracy of the g factor is about ±0.00006. [c] The accuracy of the hyperfine constants is about ±0.02 G; the accuracy of the g factor is about ±0.00003. [d] Value revised slightly from previous determination.[10]

because it is near the center of the spectrum and does not experience much CIDEP. It is also severely distorted by the signal from the irradiated silica cell (see the central portion of Figure 1 at 0 G). However, the next two major line groupings above center (corresponding to relative intensities 15 and 6 for six equivalent protons) show typical second-order splittings,[31] see Figure 2. The lines making up the high-field "intensity 15" group of lines should each be split into three lines of relative intensity 1:5:9.[31] This pattern can be seen in Figure 2. The existence of these second-order splitting patterns, associated with six equivalent protons, further supports the assignment of all of these lines to the $H_2N-{}^{\bullet}C(CH_3)_2$ radical.

The positions of the most intense second-order components (intensity 5) of the line groups centered at −44 and +34 G offset (eighteen lines total) were used to determine the parameters for this radical by a least-squares procedure that includes full diagonalization of the Hamiltonian matrix. The rms error in position between observed and calculated line positions was 0.01 G. These parameters are listed in Table 1. This spectrum is assigned to the radical, $H_2N-{}^{\bullet}C(CH_3)_2$, formed by decarboxylation. To our knowledge, this radical has not been reported earlier, even in steady-state radiolysis.

The quantum chemical calculations support the above assignment. Attempts to locate a neutral zwitterionic radical precursor formed from the α-methylalanine anion by electron loss found instead a weak complex (CC bond length ∼3 Å) between CO_2 and the neutral, carbon-centered dimethyl(aminomethyl) radical, $H_2N-{}^{\bullet}C(CH_3)_2$. The structure of the decarboxylated $H_2N-{}^{\bullet}C(CH_3)_2$ radical was optimized, and the hyperfine coupling constants were computed by the method described above. The six equivalent protons on the two methyl groups give an averaged hyperfine splitting of 18.4 G, the two equivalent protons on the NH_2 group give an averaged hyperfine splitting of 5.4 G, and the nitrogen hyperfine splitting is computed to be 2.4 G in vacuo. Only small changes in these computed values are affected by including solvent contributions from the dielectric model. The corresponding results are then 17.5, 3.6, and 1.5 G, respectively. Reoptimizing the structure of this radical in the presence of one explicit water molecule, located to act as a hydrogen bond donor to the nitrogen, produces further small shifts, to 18.9, 5.7, and 0.7 G, values in close agreement with the experimental observations (18.90, 6.07, and 1.32 G, respectively) for this radical in aqueous solution.

Direct Identification of the Aminyl Radical. Weak, broad lines are seen in the regions near −33, −12, +5, and +17 G offsets. Expanded portions of the spectrum are shown in Figures 2 and 3; Figure 4 includes three more sections. Together these portions of the spectrum represent the six line groups attributed to the aminyl radical, $HN^{\bullet}-C(CH_3)_2-CO_2^-$. (The fourth line group, going from low field to high, is partly included in Figure 2.) These line groups are spaced in a six-line pattern described by splittings for one nitrogen and one hydrogen (a_N = 13.4 and a_H = 22.3 G). Many of the lines are at least partially obscured by the stronger lines of $H_2N-{}^{\bullet}C(CH_3)_2$. Figure 2 shows lines from the aminyl radical together with some sharper lines from the $H_2N-{}^{\bullet}C(CH_3)_2$ radical that belong to the group

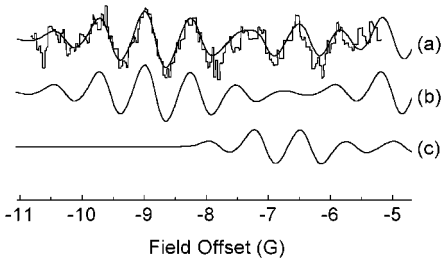

Figure 3. Spectra as in Figure 2. In b is the contribution of two line groups for the aminyl radical, and in c is that for $NH_2-C(CH_3)({}^{\bullet}CH_2)-CO_2^-$. The experimental spectrum and the sum of the two contributions is given in a.

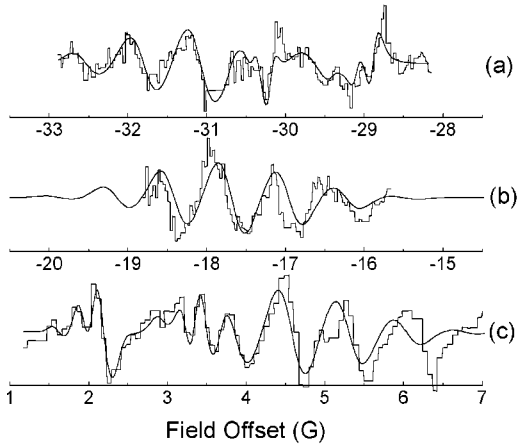

Figure 4. Spectra for three other regions of the spectrum in Figure 1. The calculated spectra include contributions from the aminyl radical as well as, in a and c, from $H_2N-{}^{\bullet}C(CH_3)_2$. The lines for the latter radical in a are inverted.

of relative intensity 15 above the center. An additional splitting of 0.7 G within the six line groups attributed to the aminyl radical is consistent with a septet produced by interaction with the six methyl protons. The parameters are summarized in Table 1. These lines are quite broad and are only slightly polarized implying short T_1 and T_2 relaxation times. (Even the group at the lowest field is in absorption and is nearly as intense as those on the high-field side of the spectrum.) Additional support for the septet form of these groups is given in the later section describing the kinetic traces.

To help confirm this assignment, predicted spectra have been added to Figures 2−4. Although the lines attributed to the aminyl radial are weak and overlapped by other lines, there is little question that the line positions are correctly identified. As is shown in Figures 2 and 3, there is also evidence of the lines of the radical $NH_2-C(CH_3)({}^{\bullet}CH_2)CO_2^-$ seen previously in the steady-state spectra.[10]

Once again the quantum chemical calculations support these experimental interpretations. The aminyl radical anion is computed to be energetically more stable by 6.2 kcal/mol than $NH_2-C(CH_3)({}^{\bullet}CH_2)CO_2^-$ in vacuo and by 2.7 kcal/mol in aqueous solution modeled as described above. Calculated

TABLE 2: Parameters Used in Modeling ESR Responses

radical	T_1[a]	T_2[a]
$SO_3^{\bullet-}$	1.5	1.5
$HN^{\bullet}-C(CH_3)_2-CO_2^-$	0.23	0.23
$H_2N-{}^{\bullet}C(CH_3)_2$	3.0	0.85
inhomogeneity parameter, ΔB_0	0.054 G	
microwave magnetic field, B_1	0.020 G @ −10 dB	

[a] Values in microseconds.

TABLE 3: Computed ^{14}N and ^{1}H Hyperfine Coupling Constants from DFT[a]

radical	nucleus	vacuo	aquo[b]
$H_2N-{}^{\bullet}C(CH_3)_2$	N	2.4	1.5
	H_N	5.4	3.6
	H_{Me}	18.4	17.5
$H_2N-C(CH_3)({}^{\bullet}CH_2)CO_2^-$	N	0.5	1.3
	H_α	−15.9	−22.2
	H_N	−1.2	−0.2
	H_{Me}	−0.9	1.8
$HN^{\bullet}-C(CH_3)_2-CO_2^-$	N	9.7	10.6
	H_α	−17.4	−20.1
	H_{Me}	−0.5	0.5

[a] Coupling constants in G from B3LYP/[5s2p1d,3s1p] calculations at the B3LYP/6-31+G(d,p) geometry. [b] Solvent effects calculated at the CPCM-B3LYP/[5s2p1d,3s1p] level, CPCM- B3LYP/6-31+G(d,p) geometry.

TABLE 4: Predicted ^{13}C Hyperfine Coupling Constants from DFT[a]

radical	nucleus	vacuo	aquo[b]
$H_2N-{}^{\bullet}C(CH_3)_2$	C_α	54.1	52.6
	C_β	−3.0	−0.7
$H_2N-C(CH_3)({}^{\bullet}CH_2)CO_2^-$	C_α	34.9	31.4
	C_β	−9.3	−10.8
	C_γ(Me)	9.6	27.9
	$C_\gamma(CO_2^-)$	18.7	11.4
$HN^{\bullet}-C(CH_3)_2-CO_2^-$	C_β	−7.4	−10.3
	C_γ(Me)	27.4	26.1
	C_γ'(Me)	−1.3	−0.9
	$C_\gamma(CO_2^-)$	16.3	17.4

[a] Coupling constants in G from B3LYP/[5s2p1d,3s1p] calculations at the B3LYP/6-31+G(d,p) geometry. [b] Solvent effects calculated at the CPCM-B3LYP/[5s2p1d,3s1p] level, CPCM- B3LYP/6-31+G(d,p) geometry.

coupling constants for $HN^{\bullet}-C(CH_3)_2-CO_2^-$ in vacuo are $a_N = +9.7$ G, $a_H = -17.4$ G (2H), and $a_H = -0.5$ G (3H), whereas in aqueous solution, the predicted values generally move closer to experiment, to +10.6, −20.1, and +0.1 G, respectively (cf 13.43, 22.30, and 0.73 G, from experiment). For $NH_2-C(CH_3)({}^{\bullet}CH_2)CO_2^-$ the solvent exerts a large influence on the splitting by the methylenic protons; the computed values move from −15.9 G in the gas phase to −22.2 G in water, with the latter in close accord with experiment (21.89 G). At nitrogen, the corresponding changes are more modest in magnitude moving from 0.5 to 1.3 G; the experiment gives 2.97 G. The averaged splitting that is due to the three methyl protons (assuming free rotation) changes from −0.9 G to +1.8 G upon solvation, which may be compared to the experimental value of 0.73 G. These values and the corresponding results for the aminyl radical anion and the decarboxylated radical are collected in Table 3. Table 4 lists predicted couplings at carbon 13 which have not been measured in this work because of the expense.

Figure 2 shows the predicted positions of the lines of the aminyl radical (b) and $NH_2-C(CH_3)({}^{\bullet}CH_2)CO_2^-$ (c) formed by abstraction of a methyl hydrogen. A composite spectrum, also including the contribution from $H_2N-{}^{\bullet}C(CH_3)_2$, is shown

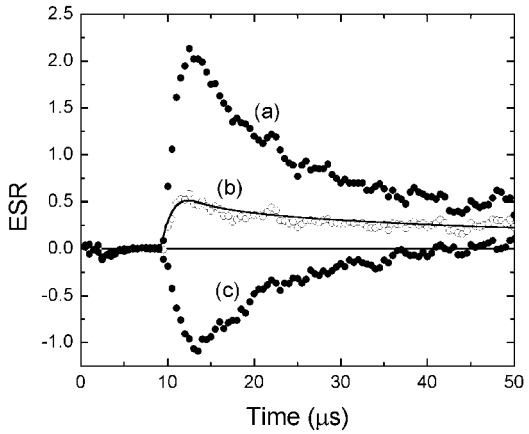

Figure 5. Time-resolved curves of ESR intensity for lines of $H_2N-{}^{\bullet}C(CH_3)_2$ at (a) high field and (c) a symmetrically located line at low field. At b is given the average of the two other curves so that the CIDEP effect is largely canceled.

overlapping the experimental trace in a. The agreement is good considering the signal-to-noise ratio. The lines from $NH_2-C(CH_3)({}^{\bullet}CH_2)CO_2^-$ make a contribution evident near 21.5 and at 15.6 G as well as affecting the relative heights in the second-order patterns of $H_2N-{}^{\bullet}C(CH_3)_2$ on the right of the spectrum. Figure 3 shows a portion of the spectrum near the center, and again, the necessity for including lines of $NH_2-C(CH_3)-({}^{\bullet}CH_2)CO_2^-$ is seen in the region around −7 G. From Figure 1, it can be seen that lines of $H_2N-{}^{\bullet}C(CH_3)_2$ should also appear in this region. No evidence is seen, so these lines must be of very little intensity as a result of CIDEP. The simulations fit the observed spectra in the three portions in Figure 4 convincingly with only some small deviations of ∼0.1 G along the field axis evident. The line positions are predicted to within the error limits suggested for the parameters in Table 1. Lines of $H_2N-{}^{\bullet}C(CH_3)_2$ can be seen in a and c and have been included in the simulation. No evidence was found for the lines of $^{\bullet}N{=}C(CH_3)_2$, which was seen in the continuous radiolysis experiment.[11] Although the lines assigned to the aminyl radical are weak and partly obscured by other lines, we believe that the assignment is, nevertheless, on strong ground.

Attempts to investigate the role of explicit solvating water molecules in modulating the observed coupling constants were again explored in each radical by reoptimizing each structure in the presence of one water molecule. In the carbon-centered radical anion, a bridging water, accepting from the amine hydrogen and donating to the carboxyl oxygen, moves each of the calculated coupling constants toward experiment, $a_N = 2.1$ G, $a_H = -21.8$ G (2 H), and $a_H = 1.4$ G (3 H). In the aminyl radical anion; however, such a bridging water moves the calculated nitrogen and amine hydrogen slightly away from experiment (to +9.8 and −18.2 G respectively), whereas the averaged splitting of the methyl H is computed at −0.6 G.

Kinetics of $H_2N-{}^{\bullet}C(CH_3)_2$ and $HN^{\bullet}-C(CH_3)_2-CO_2^-$. Kinetic traces of the ESR intensity at the center of lines of $H_2N-{}^{\bullet}C(CH_3)_2$ and $HN^{\bullet}-C(CH_3)_2-CO_2^-$ are shown in Figures 5 and 6, respectively. The curves a and c in Figure 5 show the response of an intensity 9 component (located at about 13.7 G in Figure 2) and of the symmetrically located component (also intensity 9) on the low-field side of the $H_2N-{}^{\bullet}C(CH_3)_2$ spectrum, respectively. The average of these two curves is shown at Figure 5b. The trace in Figure 6 is for the $HN^{\bullet}-C(CH_3)_2-CO_2^-$ line at −8.9 G (at the center of the septet formed by the splitting

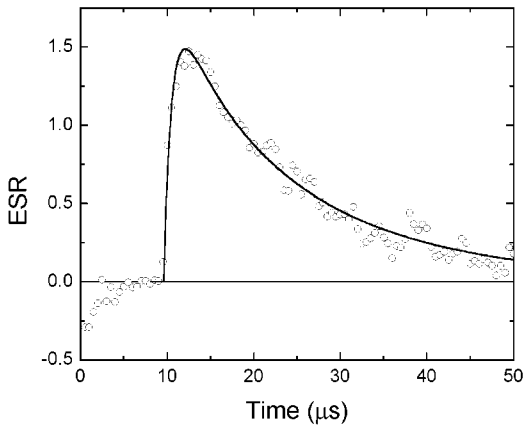

Figure 6. Time-resolved curve of ESR intensity for the line of the aminyl radical at −8.85 G. Correction has been made for a small (negative) signal of about 0.3 units from the irradiated cell.

from the methyl protons) in Figure 3. This curve has been corrected for a small, broad transient signal (presumably from the silica cell) seen at this position in the spectrum. This "baseline" was obtained by a recording at the same position and with the same field step using the solution of sulfite that is used to provide the field calibration for determining the *g* factor.

The solid curves in Figures 5 and 6 were calculated by use of modified Bloch equations using the relaxation times shown in Table 2. In both cases, the appearance of the radical was assumed to be rapid on the microsecond time scale, and the initial rise of the ESR signal agreed with that assumption. This conclusion agrees with the mechanism in the earlier study.[8] The radical $H_2N-{}^{\bullet}C(CH_3)_2$ decays moderately over the time scale displayed, whereas the radical $HN^{\bullet}-C(CH_3)_2-CO_2^-$ appears to decay mainly by a first-order process. It is of interest to compare the rate of this first-order process with that determined in the optical studies.[8] However, only an upper limit can be determined in this work because the high radical concentration makes decay by bimolecular reaction possibly also significant. If bimolecular reaction of the aminyl radicals is ignored, then the disappearance rate constant is 7×10^4 s^{-1} (lifetime of 14 μs). If there is a parallel bimolecular decay with a rate constant of 0.8×10^9 M^{-1} s^{-1} involving the total radical concentration, then a first-order rate constant of 5.5×10^4 s^{-1} fits best. The decay curves for these two calculations are very similar in shape and fit equally well considering the noise level. The solid curve in Figure 6 uses only the first-order decay. Recordings of other lines at high and low field in this spectrum show a similar decay behavior. An increase in the rate of decay of the aminyl radical by protonation involving the parent amino acid should not occur to a significant extent under the conditions used (pH 11) because little of the parent acid is in the zwitterion form.

Kinetic curves were also taken for the three lines shown at the low-field side of Figure 4a to provide support for the 0.7 G septet patterns of the line groups. These lines are not overlapped by lines from other radials, and the amplitude scaling factors should be in the intensity ratio 6:15:20 which becomes 7.4:16.2:20 after correction for overlap of the relatively broad lines. Kinetic traces with a large number of repetitions (3000) were taken at these positions, and the resultant curves were analyzed with the same parameters as those used for the curve for the aminyl radial in Figure 6. The observed scaling factors were found to be 5.7:14.3:20, in excellent agreement with the ratios expected, considering the weakness of the lines. This result supports the assignment of the fine structure to a septet.

This lifetime of 14 μs is in excellent agreement with the first-order decay constant of the aminyl radical of α-methylalanine measured from the scavenging kinetics.[8] In the scavenging experiments, the decay rate constant for the aminyl radical was determined to be 7.4×10^4 s^{-1} based on a proposed kinetic scheme. The agreement between this indirect measurement and the direct ESR measurement of the lifetime mutually support the existence of the aminyl radical and the proposed β-scission mechanism.[8] No attempt was made to detect ${}^{\bullet}CO_2^-$ because of the large line width for this radial (2.3 G)[32] and the close overlap with the line from the irradiated cell. An examination of the structure of the aminyl radical anion obtained by the DFT calculations shows an unusually long C−C bond to the carboxyl carbon (1.651 Å) and an unusually short C−N bond (1.422 Å) indicating a predisposition to β-cleavage.

Yield Measurements. An attempt was made to determine the yields of the radicals using the same approach as in the previous paper on glycine.[7] This method uses the modified Bloch equations to calculate the amplitude of the ESR time profile at the center of a line as expected from the microwave magnetic field amplitude, spin relaxation times, chemical reaction rates, and apparatus time constant. The ESR line width is taken into account implicitly through the spin relaxation times and the magnetic field inhomogeneity. Formation of the radicals is assumed to occur in <1 μs, and any delay longer than this value would readily be apparent in the rising portion of the response. Because the signals are very weak here, this method may not be of as high accuracy as in the previous case but seemed worth trying.[7] The lines used to determine the radical yields were the line of the aminyl radical near the center of that spectrum at −8.9 G in Figure 3 and the lines of $H_2N-{}^{\bullet}C(CH_3)_2$ at +13.7 and −21.5 G in Figure 2 and Figure 1, respectively. The lines of the aminyl radical are very broad corresponding to a short T_2, and probably a short T_1, so very little effect of CIDEP is seen. (The lines at low field are in absorption, and there is very little variation in amplitude of lines near the center and at positions above and below center.) The lines of $H_2N-{}^{\bullet}C(CH_3)_2$ show a large CIDEP effect, so the amplitudes of the symmetrically located lines are averaged to approximately cancel the CIDEP effect. The fact that the average is rather smaller than the individual amplitudes makes for a larger possible error in this measurement. The kinetic traces and the calculated responses are in Figures 5 and 6, respectively.

The lines of $NH_2-C(CH_3)({}^{\bullet}CH_2)CO_2^-$ were more problematic because of weakness and overlap with other lines. An estimate in this case was made by comparing the amplitudes of the first derivative lines in the synthesis in Figure 3. The line width for the radical was estimated at 0.35 G from the boxcar mode spectra. (The width is believed to arise from unresolved splitting by the nuclei of the NH_2 group.) This line width was used in the determination of the concentration relative to that of $HN^{\bullet}-C(CH_3)_2-CO_2^-$. For this case, the concentration is proportional to amplitude × width^2; the error in the relative yield could be as large as 50% because of the uncertainty in the line width. The percentage yields of the three products are given in Table 5 and add to only slightly more (104%) than the expected 100% of the ${}^{\bullet}OH$ yield as given by the amplitude found for $SO_3^{\bullet-}$. Assuming that there is no other radical of significant yield, the difference in the sum of the yields from 100% is a measure of the error in those measurements. The final values for the yields were determined as percentages by normalizing the sum of the values for the three radicals to 100%. The largest yield is found to be 59% for the aminyl radical, and the yields of decarboxylation ($H_2N-{}^{\bullet}C(CH_3)_2$) and abstraction from a

TABLE 5: Data for Reaction Yield Determinations

radical	ESR line position[a]	μ-wave power (dB)	scale factor[b]	degeneracy	yield[c]	normalized yield[c,d]
$SO_3^{\bullet-}$	−4.55	−15	10.1	1	100	100
$HN^{\bullet}-C(CH_3)_2-CO_2^-$	−8.85[e]	−5	0.32	20/384	61	59
$H_2N-{}^{\bullet}C(CH_3)_2$	−21.5, 13.6[e]	−10	0.058	18/768	23	22
$NH_2-C(CH_3)({}^{\bullet}CH_2)CO_2^-$	see text	−10			20	19

[a] Position in Gauss as in Figures 1−3. [b] Factor multiplying the calculated curve to make it fit the observed curve. [c] In % of the yield of $^{\bullet}$OH, referenced to that of $SO_3^{\bullet-}$ as 100%. [d] Normalized so the sum of the yields in the last three rows adds to 100%. [e] The amplitude of these lines have been corrected for overlap with other lines in this spectrum by use of the observed line widths.

methyl group ($NH_2-C(CH_3)({}^{\bullet}CH_2)CO_2^-$) were 22 and 19%, respectively. These values are in excellent agreement with those of 56, 25, and (by difference) 19% in the optical pulse radiolysis study.[8]

Spin Trapping in α-Methylalanine. Recently, spin-trapping techniques have been successful in identifying several radicals in glycine that have escaped direct ESR detection.[7,9] The *aci*-anion of nitromethane $CH_2{=}NO_2^-$ has proven to be useful in basic solutions where the anions of α-methylalanine are the dominant species.[25,33,34] The spin-trapping experiments in this work were done under in situ steady-state radiolysis conditions. Several conditions were used, but the most satisfactory signals were obtained with 8 mM nitromethane and 50 mM α-methylalanine at pH 12 in N_2O-saturated solutions. At 8 mM nitromethane and pH 12, not all of the hydrated electrons are scavenged by N_2O, so the $CH_3NO_2^{\bullet-}$ radical anion was easily seen.[25] The $^{\bullet}$OH adduct radical $HO-CH_2-NO_2^{\bullet-}$, was also easily seen.[25] There were some small lines corresponding to radical adducts with the ≈25 G nitrogen triplet splitting and the 10 G CH_2 triplet. However, these lines were difficult to assign mainly because the lines for the $^-O_2C-CH_2-NO_2^{\bullet-}$ radical were so intense.[25] This $^{\bullet}CO_2^-$ adduct had the most intense lines in the spectrum.

The large intensity of the lines of $^-O_2C-CH_2-NO_2^{\bullet-}$ from the reaction of $^{\bullet}CO_2^-$ with $CH_2{=}NO_2^-$ is of particular note. Also of interest is the contrasting behavior of the $CH_2{=}NO_2^-$ spin trap in conjunction with the radiolysis of solutions of glycine and α-methylalanine anions. In glycine, no $^-O_2C-CH_2-NO_2^{\bullet-}$ was identified, but the aminyl radical, $HN^{\bullet}-CH_2-CO_2^-$, of the glycine anion was seen prominently as a spin adduct with $CH_2{=}NO_2^-$. The opposite is true for the $^-O_2C-CH_2-NO_2^{\bullet-}$ adduct in solutions of α-methylalanine and its corresponding aminyl radical's spin adduct. These observations are consistent with the expected propensity for α-methylalanine's aminyl radical $HN^{\bullet}-C(CH_3)_2-CO_2^-$ to undergo β scission as opposed to glycine's aminyl radical $HN^{\bullet}-CH_2-CO_2^-$.[8] The formation of $CH_2{=}NO_2^-$ spin adducts are usually not diffusion controlled;[34] for instance, its rate constant for trapping $^{\bullet}CO_2^-$ is 1.4×10^7 M^{-1} s^{-1}.[34] Thus, with the measured lifetime of 14 μs for $HN^{\bullet}-C(CH_3)_2-CO_2^-$ from β scission, the reactions of this aminyl radical with the spin trap do not appear to be competing effectively with the intramolecular β-scission process, so the rate constant for the reaction of the aminyl radical with $CH_2{=}NO_2^-$ would be $<(14\ \mu s \times 8\ mM)^{-1} = 9 \times 10^6$ M^{-1} s^{-1}. On the other hand, observation of spin adducts of the aminyl radical $HN^{\bullet}-CH_2-CO_2^-$ in solutions of glycine anions indicates that β scission is not competing with the spin trap $CH_2{=}NO_2^-$ for the aminyl radical in that case. However, 5,5-dimethyl-1-pyrroline-*N*-oxide has been used to trap $^{\bullet}CO_2^-$ in glycine,[9] which is consistent with β scission also occurring in aminyl radicals from glycine anions but at a slower rate than in aminyl radicals from anions of α-methylalanine.[8] Finally, the β-scission reaction for $HN^{\bullet}-C(CH_3)_2-CO_2^-$ (reaction 5) produces the imine, $HN{=}C(CH_3)_2$, which may be the source of the secondary product radical, $^{\bullet}N{=}C(CH_3)_2$, seen previously in steady-state experiments.[10,11]

Conclusions

Two new radicals, $HN^{\bullet}-C(CH_3)_2-CO_2^-$ and $H_2N-{}^{\bullet}C(CH_3)_2$, were identified in the $^{\bullet}$OH oxidation of α-methylalanine in aqueous solution. Direct observation of the time-resolved ESR spectra on the time scale of the radiolysis pulse suggests that both radicals are formed in the primary attack of $^{\bullet}$OH on α-methylalanine. Aminyl radicals, without special substitution at the nitrogen, appear to be rarely if ever seen in solution. Even in this case, the lines of the aminyl radical are broad, but direct identification is facilitated because of the large yield of aminyl radicals as apparently enhanced by an alkyl-substituent effect. The methyl substituents hinder facile formation of carbon-centered radicals in contrast to the easily abstracted hydrogens on the alpha carbon in glycine. Furthermore, the electron-donating properties of the methyl groups may enhance the $^{\bullet}$OH attack at the nitrogen atom. The direct observation of the first-order decay of the aminyl radical, $HN^{\bullet}-C(CH_3)_2-CO_2^-$, and the observation of $^{\bullet}CO_2^-$ spin adducts with $CH_2{=}NO_2^-$ support the contention that β scission is prominent in the chemistry of this aminyl radical. Strong support for these findings has been provided by the quantum chemical DFT calculations.

Acknowledgment. This work was supported by the Office of Basic Energy Sciences of the U.S. Department of Energy (Document No. NDRL-4344 from the Notre Dame Radiation Laboratory). P.W. thanks the International Atomic Energy Agency for a predoctoral fellowship. We also thank Dr. Marija Bonifacic for reading the manuscript and a number of helpful suggestions.

References and Notes

(1) Meisel, D.; Camaioni, D.; Orlando, T. In *ACS Symposium Series*; American Chemical Society: Washington, DC, 2001; Vol. 778, pp 342−361.
(2) Berlett, B.; Stadtman, E. R. *J. Biol. Chem.* **1997**, *272*, 20313−20316.
(3) Schöneich, C. *Exp. Gerontol.* **1999**, *34*, 19−34.
(4) Bonifacic, M.; Stefanic, I.; Hug, G. L.; Armstrong, D. A.; Asmus, K.-D. *J. Am. Chem. Soc.* **1998**, *120*, 9930−9940.
(5) Armstrong, D. A.; Rauk, A.; Yu, D. *J. Chem. Soc., Perkin Trans. 2* **1995**, 553−560.
(6) Hug, G. L.; Carmichael, I.; Fessenden, R. W. *J. Chem. Soc., Perkin Trans. 2* **2000**, 507−508.
(7) Hug, G. L.; Fessenden, R. W. *J. Phys. Chem. A* **2000**, *104*, 7021−7029.
(8) Bonifacic, M.; Armstrong, D. A.; Carmichael, I.; Asmus, K.-D. *J. Phys. Chem. B* **2000**, *104*, 643−649.
(9) Taniguchi, H.; Madden, K. P. *J. Phys. Chem. A* **1998**, *102*, 6753−6759.
(10) Neta, P.; Fessenden, R. W. *J. Phys. Chem.* **1971**, *75*, 738−748.
(11) Fessenden, R. W. *Chem. Phys. Lett.* **1974**, *29*, 364−367.
(12) Asmus, K.-D.; Stefanic, I.; Bonifacic, M.; Armstrong, D. A. Private communication.
(13) Danen, W. C.; Neugebauer, F. A. *Angew. Chem., Int. Ed.* **1975**, *14*, 783−9.
(14) Wardman, P.; Smith, D. R. *Can. J. Chem.* **1971**, *49*, 1869.

(15) Wardman, P.; Smith, D. R. *Can. J. Chem.* **1971**, *49*, 1880.
(16) Ayscough, P. B.; Mach, K. *J. Chem Soc. Faraday Trans. 1* **1972**, 1139.
(17) Kaba, R. A.; Ingold, K. U. *J. Am. Chem. Soc.* **1976**, *98*, 7375−80.
(18) Behar, D.; Fessenden, R. W. *J. Phys. Chem.* **1974**, *78*, 1074−8.
(19) Duncanson, I. B. *Fusion* **1993**, *XL*, 26.
(20) Verma, N. C.; Fessenden, R. W. *J. Chem. Phys.* **1976**, *65*, 2139−2155.
(21) Fessenden, R. W.; Hornak, J. P.; Venkataraman, B. *J. Chem. Phys.* **1981**, *74*, 3694−3704.
(22) Madden, K. P.; McManus, H. J. D.; Fessenden, R. W. *Rev. Sci. Instrum.* **1994**, *65*, 49−57.
(23) Fessenden, R. W. *J. Chem. Phys.* **1973**, *58*, 2489−2500.
(24) Fessenden, R. W. In *Chemically Induced Magnetic Polarization*; Muus, L. T., Atkins, P. W., McLauchlan, K. A., Pedersen, J. B., Eds.; D. Reidel Publishing Co.: Dordrecht, The Netherlands, 1977; pp 119−150, see Figure 3.
(25) Behar, D.; Fessenden, R. W. *J. Phys. Chem.* **1972**, *76*, 1710−1721.
(26) Becke, A. D. *J. Chem. Phys.* **1993**, *98*, 5648−5652.
(27) Hariharan, P. C.; Pople, J. A. *Chem. Phys. Lett.* **1972**, *16*, 217−9.
(28) Frisch, M. J.; Trucks, G. W.; Schlegel, H. B.; Scuseria, G. E.; Robb, M. A.; Cheeseman, J. R.; Zakrzewski, V. G.; Montgomery, J. A., Jr.; Stratmann, R. E.; Burant, J. C.; Dapprich, S.; Millam, J. M.; Daniels, A. D.; Kudin, K. N.; Strain, M. C.; Farkas, O.; Tomasi, J.; Barone, V.; Cossi, M.; Cammi, R.; Mennucci, B.; Pomelli, C.; Adamo, C.; Clifford, S.; Ochterski, J.; Petersson, G. A.; Ayala, P. Y.; Cui, Q.; Morokuma, K.; Malick, D. K.; Rabuck, A. D.; Raghavachari, K.; Foresman, J. B.; Cioslowski, J.; Ortiz, J. V.; Stefanov, B. B.; Liu, G.; Liashenko, A.; Piskorz, P.; Komaromi, I.; Gomperts, R.; Martin, R. L.; Fox, D. J.; Keith, T.; Al-Laham, M. A.; Peng, C. Y.; Nanayakkara, A.; Gonzalez, C.; Challacombe, M.; Gill, P. M. W.; Johnson, B. G.; Chen, W.; Wong, M. W.; Andres, J. L.; Head-Gordon, M.; Replogle, E. S.; Pople, J. A. *Gaussian 98*, revision A.7; Gaussian, Inc.: Pittsburgh, PA, 1998.
(29) Klamt, A.; Schüürmann, G. *J. Chem. Soc., Perkin Trans. 2* **1993**, 799−805.
(30) Carmichael, I. *J. Phys. Chem.* **1993**, *97*, 1789−92.
(31) Fessenden, R. W. *J. Chem. Phys.* **1962**, *37*, 747−750.
(32) Chawla, O. P.; Fessenden, R. W. *J. Phys. Chem.* **1975**, *79*, 2693−2700.
(33) Eiben, K.; Fessenden, R. W. *J. Phys. Chem.* **1968**, *72*, 3387−3393.
(34) Madden, K. P.; Taniguchi, H.; Fessenden, R. W. *J. Am. Chem. Soc.* **1988**, *110*, 2753−2758.